Chapter 2

Magnetovariational Method in Deep Geoelectrics

Mark N. Berdichevsky[1], Vladimir I. Dmitriev, Nina S. Golubtsova, Natalia A. Mershchikova, and Pavel Yu. Pushkarev
Faculty of Geology, Lomonosov Moscow State University, Moscow, Russia

Chapter Outline

2.1 Introduction 23
2.2 On Integrated Interpretation of MV and MT Data 26
2.3 Model Experiments 29
2.4 MV–MT Study of the Cascadian Subduction Zone (EMSLAB Experiment) 34
Acknowledgments 45
References 45

2.1 INTRODUCTION

Deep geoelectric studies of the Earth's crust and upper mantle include two methods: (1) the magnetotelluric (MT) method using the electric and magnetic fields and (2) the magnetovariational (MV) method using only the magnetic field.

Following a common practice, a leading part belongs to the MT method with impedance tensor $\hat{Z}$ and apparent resistivity ρ_a (vertical stratification of the medium, geoelectric zoning, mapping of underground topography, detection of conductive zones in the Earth crust and upper mantle, recognition of deep faults), whereas the MV method with tipper vector $\mathbf{W}$ and horizontal magnetic tensor $\hat{M}$ helps in tracing of horizontal conductivity contrasts, localization of geoelectric structures, determination of their strike. Such a partition of MT and MV methods is reflected even in the MT nomenclature: if the MT studies are referred to as MT soundings, the MV studies are considered as MV profiling (Rokityansky, 1982).

The MT–MV geoelectric complex is widely and rather successfully used throughout the world. It provides unique information on the Earth's interior (porosity, permeability, graphitization, sulfidizing, dehydration, melting, fluid regime, ground-water mineralization, rheological characteristics, thermodynamic, and geodynamic processes).

[1]Deceased.

Electromagnetic Sounding of the Earth's Interior: Theory, Modeling, Practice
http://dx.doi.org/10.1016/B978-0-444-63554-9.00002-7

The weak point of deep geoelectrics with MT priority is that inhomogeneities in the uppermost layers may severely distort the electric field and consequently the impedance tensor along with the apparent resistivity. The distortions are of galvanic nature – they extend over the whole range of low frequencies causing static ("conformal") shifts of the low-frequency branches of apparent resistivity curves. The near-surface inhomogeneities affect the apparent resistivities, no matter how low the frequency is. They spoil the information on the deep conductivity. There is a plethora of techniques for correcting these distortions. But all these techniques are fraught with information losses or even with subjective (sometimes erroneous) decisions resulting in false structures.

We can considerably improve the MT–MV complex by realizing to the full extent the potentialities of the MV method. The generally recognized advantage of MV method is that with lowering frequencies the induced currents penetrate deeper and deeper into the Earth, so that their magnetic field and consequently the tipper and magnetic tensor are less and less distorted by subsurface inhomogeneities and convey more and more information about buried inhomogeneities. This remarkable property of the magnetic field gives us the chance to protect the deep geoelectric studies from the static-shift problem (no electric field is measured). But excluding the electric field, we face the problem of informativeness of the MV method. It is commonly supposed that "MV studies determine only horizontal conductivity gradients, while the vertical conductivity distribution is not resolved" (Simpson and Bahr, 2005). Is it true? The fallacy of this statement is clearly seen from Figure 2.1, which shows a two-dimensional (2-D) model

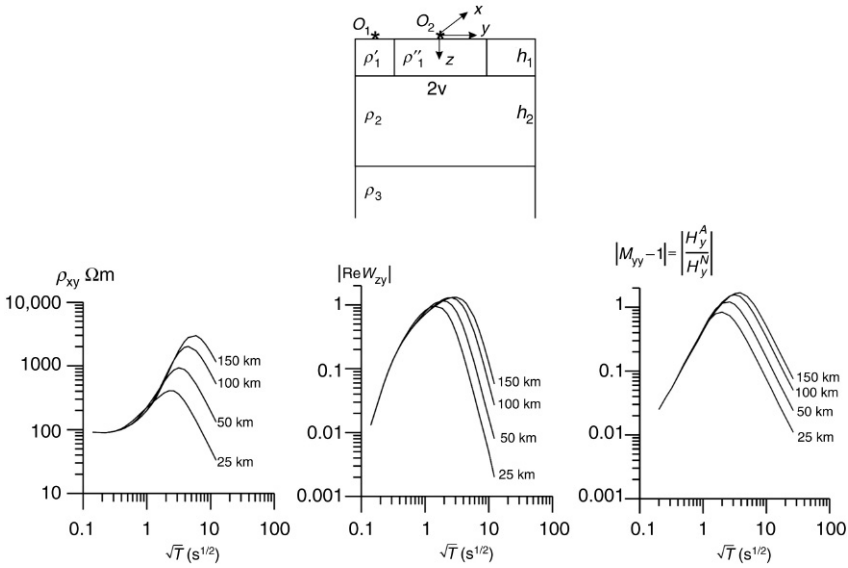

FIGURE 2.1 Illustrating the resolution of MT and MV soundings. Model parameters: $\rho_1' = 100\,\Omega$m, $\rho_1'' = 10\,\Omega$m, w = 8 km, h_1 = 1 km, ρ_2 = 10,000 Ωm, h_2 = 24, 49, 99, 149 km, ρ_3 = 1 Ωm. Curve parameter: $h = h_1 + h_2$.

with an inclusion of higher conductivity in the upper layer resting on the resistive strata and conductive basement. The half width of the inclusion is 8 km. A depth to the conductive basement ranges from 25 km to 150 km. Let us compare the longitudinal apparent resistivity curves ρ_{xy} measured outside the inclusion (site O_1, $y = -9$ km), with the real-tipper curves $\left|\mathrm{Re}\,W_{zy}\right| = \left|\mathrm{Re}\left(H_z^a / H_y\right)\right|$, measured at the same site O_1, and with the magnetic-tensor curves $\left|M_{yy} - 1\right| = \left|\mathrm{Re}\left(H_y^a / H_y^n\right)\right|$, measured inside the inclusion (site $O_2, y = 0$). In the model under consideration, the bell-shaped MV curves $\left|\mathrm{Re}\,W_{zy}\right|$ and $\left|M_{yy} - 1\right| = \left|\mathrm{Re}\left(H_y^a / H_y^n\right)\right|$, derived from the ratio between the vertical component of the anomalous magnetic field to the horizontal component of the magnetic field and from the ratio between the horizontal component of the anomalous magnetic field to the horizontal component of the normal magnetic field, resolve the vertical conductivity distribution no worse than the customary MT curves ρ_{xy}. Generalizing these indications, we can say that the MV method reveals not only horizontal variations in the Earth's conductivity but the vertical variations as well. Moreover, we can appeal to the uniqueness theorem proved by Dmitriev for 2-D tipper and 2-D horizontal magnetic tensor and state that the 2-D piecewise analytical distribution of conductivity is uniquely defined by exact values of the tipper or the horizontal magnetic tensor given over all points of infinitely long transverse profile in the entire range of frequencies from 0 to ∞ (Berdichevsky et al., 2003; Dmitriev and Berdichevsky, Chapter 7, this volume). The physical meaning of this unexpected result is rather simple. Naturally, the MV studies of horizontally homogeneous media with zero MV anomalies make no sense. But in the case of the horizontally inhomogeneous medium, the MV studies can be considered as ordinary frequency soundings using the magnetic field of excess currents distributed within a local horizontal inhomogeneity, which plays a role of the buried source.

So, we have every reason to revise the traditional MT–MV complex and consider a new MV–MT complex, within which the MV method, as being tolerant to subsurface distortions, plays a leading part and gives a sound geoelectric basis for MT-detailed specification. This approach goes back to the MT experiments that were performed in 1988–1990 in the Kirghiz Tien Shan mountains by geophysical teams of the Institute of High Temperatures, Russian Academy of Sciences (Trapeznikov et al., 1997; Berdichevsky and Dmitriev, 2002). These measurements were carried out at a profile characterized by strong local and regional distortions of apparent resistivities that dramatically complicated the interpretation of resulting data. The situation has normalized only with MV soundings. Figure 2.2 shows the real tippers, $\mathrm{Re}W_{zy}$, and the geoelectric model fitting these observation data. The model contains an inhomogeneous crustal conductive layer (a depth interval of 25–55 km) and vertical conductive zones confined to the known faults, the Nikolaev line (NL) and the Atbashi-Inylchik fault (AIF). The figure also presents the model reconstructed from seismic tomography data. The geoelectric model agrees remarkably well with the seismic model: low resistivities correlate with lower velocities. This correlation confirms the validity of geoelectric reconstructions based on MV data. We see that MV soundings not only outline crustal conductive zones but also stratify the lithosphere.

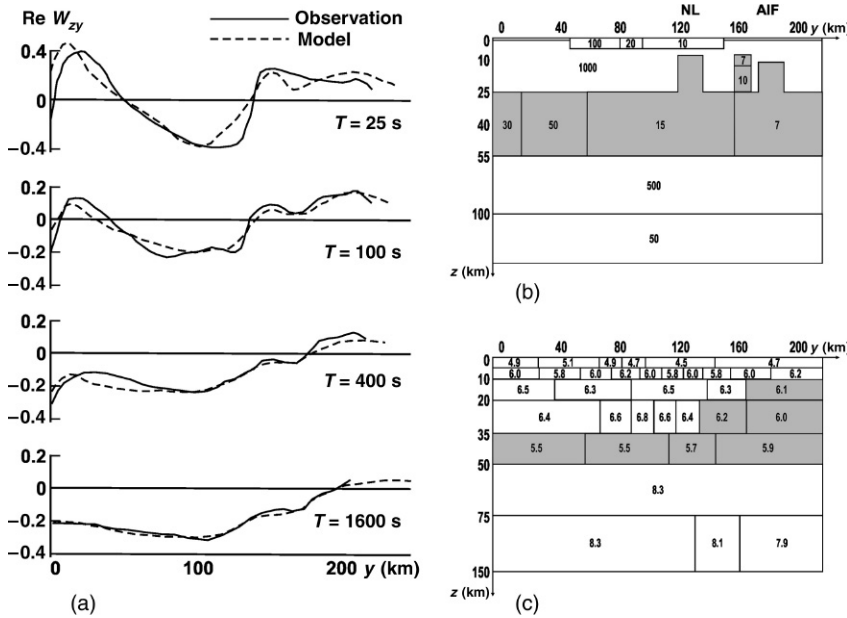

FIGURE 2.2 Magnetovariational sounding in the Kyrgyz Tien Shan Mountains. (a) Plots of the real tipper along a profile crossing the Kyrgyz Tien Shan. (b) The resistivity section from MV data (Trapeznikov et al., 1997): NL, Nikolaev line; AIF, Atbashi-Inylchik fault. The resistivity values in Ωm are given within blocks; the lower-resistivity crustal zone is shaded. (c) The velocity section from seismic tomography data (Roecker et al., 1993). Values of *P* wave velocities in kilometers per second are given within blocks; the low-velocity crustal zone is shaded.

The advancement of the MV–MT complex with MV priority is facilitated by the emergence of codes combining MV and MT automatized inversions (Siripunvaraporn and Egbert, 2000; Nowozynski and Pushkarev, 2001; Varentsov, 2002).

Our paper is devoted to strategy of integrated MV and MT inversions. We consider general questions of MV–MT complex, describe model experiments on synthetic data and present a new model of the Cascadian subduction zone constructed with MV priority.

2.2 ON INTEGRATED INTERPRETATION OF MV AND MT DATA

The inverse problem of MV and MT soundings is unstable. An arbitrarily small error in the measurement data can give rise to an arbitrarily large error in the conductivity distribution. Such a problem is meaningful if we use a priori information and limit the parameters to be found so that an approximate solution of the inverse problem is sought within a compact set of plausible solutions forming an interpretation model.

An interpretation model should reflect current notions and hypotheses as to the sediments, crust, and upper mantle. It can either smooth or emphasize geoelectric contrasts and incorporate inhomogeneous layers and local inclusions of higher or lower electric conductivity. An approximate solution of an inverse problem constrained by the interpretation model is chosen by criteria ensuring the agreement of the solution with the available a priori information and observations. The number of such criteria is defined by the number of response functions in use (real and imaginary or amplitude and phase functions). If a few response functions are used in the inversion, the problem is referred to as multicriterion.

The 2-D integrated interpretation of MV and MT data belongs to the class of multicriterion problems. The electric conductivity of the Earth can be determined from the TE mode with the response functions $\mathrm{Re}W_{zy}$, $\mathrm{Im}W_{zy}$, $\rho^{\parallel}$, and $\varphi^{\parallel}$ (real and imaginary tippers, longitudinal apparent resistivities and phases of longitudinal impedances) and from the TM mode with the response functions $\rho^{\perp}$ and $\varphi^{\perp}$ (transverse apparent resistivities and phases of transverse impedances). These functions differ in sensitivity to target geoelectric structures and in stability with respect to subsurface distortions (Berdichevsky and Dmitriev, 2002). The TE mode is more sensitive to deep conducting structures and less sensitive to the resistance of the lithosphere, whereas the TM-mode is less sensitive to deep conducting structures and more sensitive to the resistance of the lithosphere. Also note that apparent resistivities over the entire range of low frequencies can be subject to strong static distortions due to local three-dimensional (3-D) subsurface inhomogeneities (geoelectric noise), whereas low-frequency tippers and impedance phases are free from these distortions. An algorithm of the 2-D bimodal inversion should implement such a procedure that the used characteristics would support and complement each other: gaps arising in the inversion of one response function should be filled through the inversion of another. In inverting various characteristics, one should give priority to the most reliable elements of the model and suppress the least reliable ones.

The following two approaches are possible in solving multicriterion inverse problems: (1) parallel (joint) inversion of all characteristics used and (2) successive (partial) inversions of each of the characteristics.

The parallel inversion summarizes all inversion criteria related to various response functions. In the 2-D problem, it reduces to the minimization of the Tikhonov's functional

$$\inf_{\mathbf{p}} \left\{ \sum_{m=1}^{M} \gamma_m \left| \left| F_m(y,\omega) - I_m(\sigma) \right| \right|^2 + \alpha\Omega(\sigma) \right\} \tag{2.1}$$

where the following notation is used: $\mathbf{p}$, vector of the sought-for parameters; F_m, response function in use; y, coordinate of the observation point; ω, frequency; I_m, operator determining F_m from the known distribution of the conductivity σ; γ_m, significance coefficient of the model misfit (deviation of I_m from F_m); Ω,

criterion of solution selection (stabilizer) adjusting the solution to a priori information; α, regularization parameter (the significance coefficient of the prior information); M, number of the response functions used.

At first glance, the parallel inversion seems to be most effective because it incorporates all the specific features of the multicriterion problem together and significantly simplifies the work of the geophysicist.

However, this approach is open to criticism. If various characteristics F_m have the same sensitivity to all parameters $\mathbf{p}$ (p_1, p_2, … p_S) of the geoelectric structure and the same immunity to subsurface distortions, their parallel inversion is not very advantageous because only a single one, the most reliably determined, characteristic is sufficient for a comprehensive inversion.

The use of several characteristics F_m makes the inversion more informative if they differ significantly in their sensitivity to various parameters of the geoelectric structure and in their immunity to distortions. However, in this case, their joint inversion can become inconsistent, because they put different constraints on the geoelectric structure and are related to different criteria of model misfits and solution selection. Clearly, they can interfere with one another. True enough, it is possible that in some cases a fortunate choice of weights allows one to construct a self-consistent model with a small overall misfit. However, the adequate selection of such weights is itself a complex problem that often cannot be solved as yet. Apparently, the SPI method (successive partial inversions) is the best approach to the solution of a multicriterion inverse problem.[1]

Let a response function F_m be the most sensitive to the vector of parameters $\mathbf{p}^{(m)}$. Then, the partial mth inversion of the multicriterion 2-D problem consists in the minimization of the following Tikhonov's functional on the set of the parameters $\mathbf{p}^{(m)}$, with other parameters being fixed:

$$\inf_{\mathbf{p}^{(m)}} \left\{ \left\| F_m(y,\omega) - I_m(\sigma) \right\|^2 + \alpha\Omega(\sigma) \right\} \tag{2.2}$$

The successive application of the functions F_m, $m = 1, 2, \ldots, M$ reduces the solution of the multicriterion problem to a succession of partial inversions. Each partial inversion is intended for the solution of a specific problem and can be restricted to specific structures.

A decrease in the number of parameters minimizing the Tikhonov's functional significantly enhances the stability of the problem. Partial inversions comprehensively incorporate specific features of the response functions used, their informativeness, and their confidence intervals. They allow the information exchange between various functions, enable a convenient interactive dialog,

1. It is worth mentioning that due to nonlinearity and incorrectness of the inverse problem solution, the result of the successive partial inversions (2.2) not necessarily should agree with the result of the parallel inversion (2.1): generally speaking, they are two different statements of the inverse problem solution. By the same reason, the results of two different sequences of the same partial inversions of the initial data may be different.

and are easily tested. We believe that this direction of research is most promising for further development of methods designed for the integrated interpretation of MV and MT data.

The method of partial inversions is corroborated by results of studies carried out in various geological provinces (Trapeznikov et al., 1997; Berdichevsky et al., 1998, 1999; Pous et al., 2001; Vanyan et al., 2002). We briefly describe some model experiments elucidating the potentials of SPI with MV priority.

2.3 MODEL EXPERIMENTS

Figure 2.3 displays a 2-D model schematically illustrating geoelectric structure of the Kyrgyz Tien Shan (Trapeznikov et al., 1997). This model, referred as the TS model, includes (1) inhomogeneous sediments, (2) inhomogeneous resisting crust, (3) deep crustal layer with a resistivity increasing monotonically from 10 Ωm in the south to 300 Ωm in the north, (4) three conducting zones A–C branching from the crustal conducting layer, and (5) a poorly conducting mantle underlain by a conducting asthenosphere at a depth of 150 km. The model is excited by a vertically incident plane wave.

The forward problem was solved with the use of the finite element method (Wannamaker et al., 1987). Gaussian white noise was added to the response functions: it had 5% standard deviations for longitudinal and transverse apparent resistivities $\rho^{\parallel}$ and $\rho^{\perp}$, 2.5° for phases of longitudinal and transverse impedances $\varphi^{\parallel}$ and $\varphi^{\perp}$, and 5% for real and imaginary parts of the tipper $\mathrm{Re}W_{zy}$ and $\mathrm{Im}W_{zy}$. To simulate the static shift caused by small 3-D near-surface inhomogeneities,

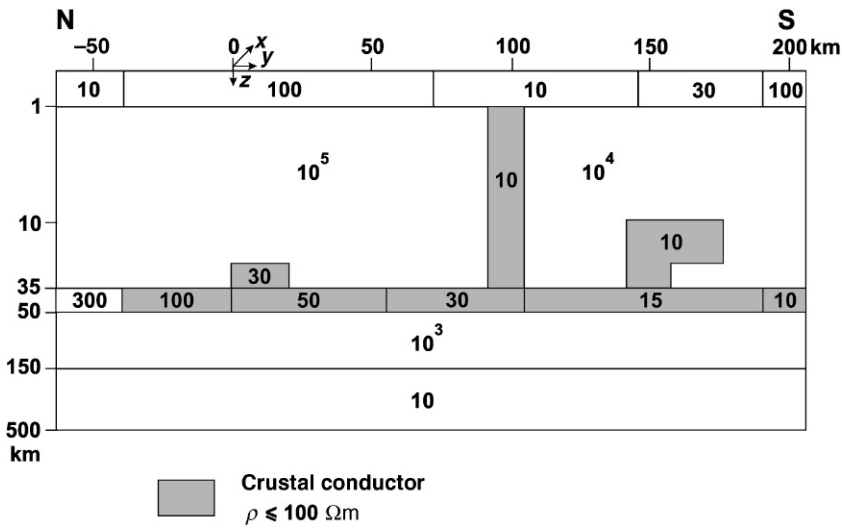

FIGURE 2.3 The TS model. The resistivity values in Ωm are shown within blocks; blocks of lower crustal resistivities are shaded.

the apparent resistivities were multiplied by random real numbers uniformly distributed in the interval from 0.5 to 2.

The integrated interpretation of the synthetic data obtained in the TS model was performed by the method of partial inversions.

The construction of the interpretation model is the most important step of interpretation (Berdichevsky and Dmitriev, 2002). The interpretation model should meet the following two requirements: it should be informative (i.e., reflect the target layers and structures) and it should be simple (i.e., be determined by a small number of parameters ensuring the stability of the inverse problem).

It is evident that these requirements are antagonistic: a more informative model is more complex. Therefore, an optimal model, both simple and informative enough, should be chosen. This is a key point of the interpretation, defining the strategy and even, to an extent, the solution of the inverse problem. The choice of the interpretation model is restrained by a priori information, qualitative estimates, and reasonable hypotheses on the structure of the medium under study.

Constructing the interpretation model for inversions of the synthetic data in the TS model, we assumed that the following a priori information on the studied medium was available: (1) the sedimentary cover is inhomogeneous, with an average thickness of 1 km, (2) the consolidated crust is inhomogeneous and can contain local conducting zones, its resistivity can experience regional variations, and an inhomogeneous conducting layer corresponding to the seismic waveguide can exist in its lower part at depth of 35–50 km, (3) the upper mantle consists of homogeneous layers, and its resistivity at depths below 200 km can amount to 20 Ωm, and (4) the area under observation is framed by asymmetric media which slowly vary with distance.

To detail these assumptions, we inverted the tippers using a smoothing code capable of identifying and localizing crustal conductors. We applied the REBOCC code (Siripunvaraporn and Egbert, 2000) and use a homogeneous half-space with a resistivity of 100 Ωm as an initial approximation. Figure 2.4 presents this trial model, resulting from the inversion of $\mathrm{Re}W_{zy}$ and $\mathrm{Im}W_{zy}$. The model yields clear evidence of three local crustal conducting zones A – C ($\rho < 30$ Ωm branching from the crustal conducting layer) but fails to stratify the crust and upper mantle.

The prior information complemented with data on local crustal conductors provides a reasonable basis for the construction of a block interpretation model. This model, presented in Figure 2.5, consists of 70 blocks of a fixed geometry and different starting resistivities. The partition density depends on the position and size of tentative structures and is highest within the sedimentary cover, local crustal conductors, and crustal conducting layer.

Partial inversions of the synthetic data were performed in the class of block structures with the use of the II2DC code (Varentsov, 2002) in the following succession: (1) $\mathrm{Re}W_{zy}$ and $\mathrm{Im}W_{zy}$ inversion, (2) $\varphi^{\parallel}$ inversion, and (3) $\rho^{\perp}$ and $\varphi^{\perp}$ inversion. All the inversions were carried out automatically. We consider each inversion separately.

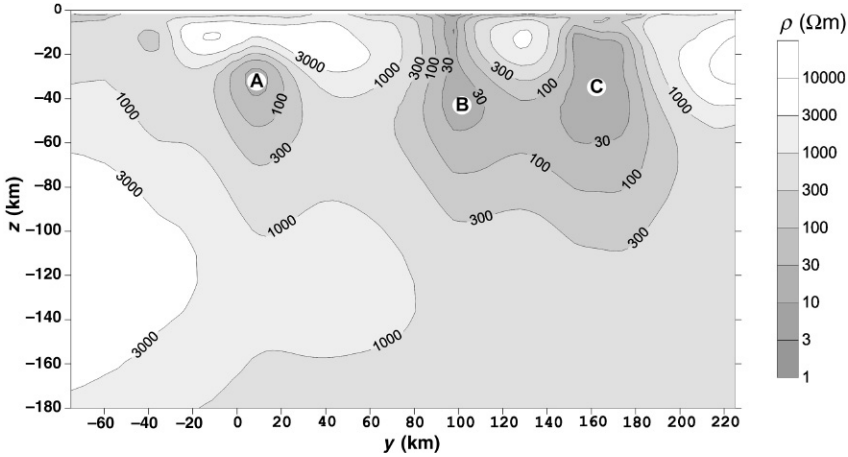

FIGURE 2.4 The trial model: Inversion of ReW_{zy} and ImW_{zy} using the REBOCC code; A–C are conducting zones in the crust (cf. Figure 2.3).

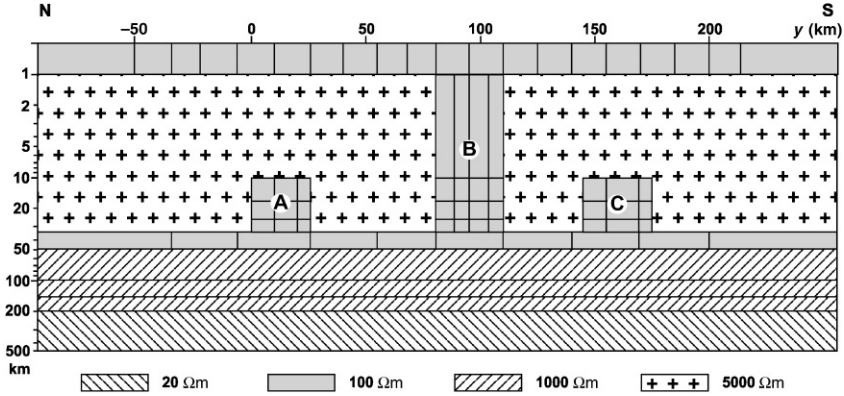

FIGURE 2.5 The interpretation block model; starting values of resistivities in Ωm are shown within blocks.

1. Inversion of ReW_{zy} and ImW_{zy}. The starting model is shown in Figure 2.5. The tipper inversion results in the TP model (Figure 2.6), which agrees well with the initial TS model. The divergence between the tippers calculated from both models is generally no higher than 5–7% within the period range from 1 s to 10,000 s. Using the MV data alone, we successfully reconstructed the most significant elements of the initial model, including the inhomogeneous sedimentary cover; the local crustal conductors A–C; and the inhomogeneous crustal conducting layer whose resistivity varies from 234 Ωm in the north to 16 Ωm in the south (from 300 Ωm to 10 Ωm in the initial model). Also resolved was the contrast between the nonconductive and conductive

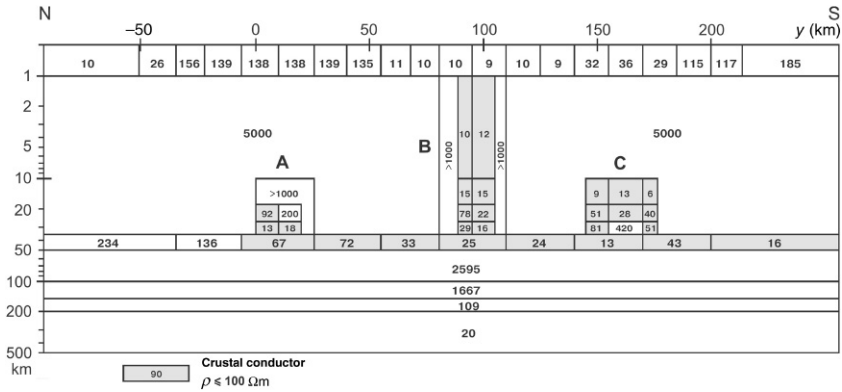

FIGURE 2.6 The TP model: Inversion of $\mathrm{Re}W_{zy}$ and $\mathrm{Im}W_{zy}$ using the II2DC code; the resistivity values in Ωm are shown within blocks; blocks of lower crustal resistivities are shaded (cf. Figure 2.3).

mantle (1667 Ωm/109 Ωm in the TP model against 1000 Ωm/10 Ωm in the initial TS model). We see that the MV response functions measured on a 200 km profile allowed us not only to detect the local conducting zones but also to determine the stratification of the medium (with an accuracy sufficient for obtaining gross petrophysical estimates).

2. Inversion of $\varphi^{\parallel}$. At this step, without going beyond the TE mode, we can control the tipper inversion and gain additional constraints on the stratification of the medium. A difficulty consists in the fact that the $\rho^{\parallel}$ curves of the longitudinal apparent resistivity are distorted by subsurface 3-D inhomogeneities that create geoelectric noise. We avoided this difficulty by confining ourselves to the inversion of the undistorted $\varphi^{\parallel}$ curves. If $\rho^{\parallel}$ and $\varphi^{\parallel}$ are interrelated through dispersion relations, the disregard of the $\rho^{\parallel}$ curves does not lead to a loss of information. We interpreted the $\varphi^{\parallel}$ curves using the TP model, obtained from the tipper inversion, as a starting model. Inversion of $\varphi^{\parallel}$ resulted in the TE model, shown in Figure 2.7. The divergences between the phases from the TE model and initial TS model do not exceed 2.5°. Comparing the TE and TP models, we see that the phase inversion agrees reasonably well with the tipper inversion. Two points are of particular interest: (1) the edge resistivities of the inhomogeneous crustal layer (343 and 10 Ωm) became closer to their true values (300 and 10 Ωm), and (2) the contrast between the nonconductive and conductive mantle became sharper (3801 Ωm/15 Ωm in the TE model against 1000 Ωm/10 Ωm in the initial TS model). Thus, the phase inversion visibly improved the accuracy of the medium stratification.
3. Inversion of $\rho^{\perp}$ and $\varphi^{\perp}$. This inversion is sensitive to galvanic effects. It is focused on estimating the resistivity of the upper highly resistive crust. The TE model, obtained from the inversion, was used as a starting model. Here, we fixed all resistivities except for blocks that contact the sedimentary cover.

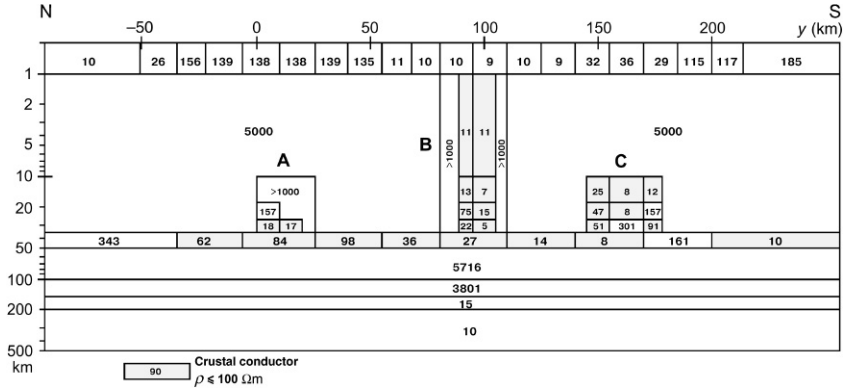

FIGURE 2.7 The TE model: Inversion of $\varphi^{\parallel}$ using the II2DC code; the resistivity values in Ωm are shown within blocks; blocks of lower crustal resistivities are shaded (cf. Figure 2.3).

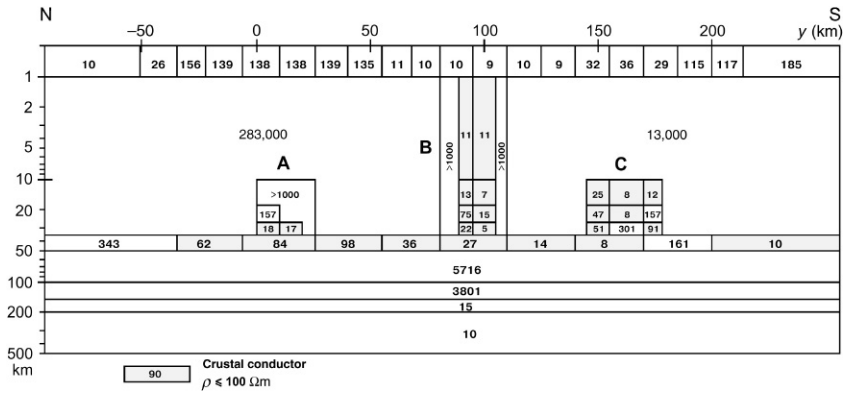

FIGURE 2.8 The TM model: Inversion of $\rho^{\perp}$ and $\varphi^{\perp}$ using the II2DC code; the resistivity values in Ωm are shown within blocks; blocks of lower crustal resistivities are shaded (cf. Figure 2.3).

The inversion of $\rho^{\perp}$ and $\varphi^{\perp}$ yielded the TM model, shown in Figure 2.8. It confirms the galvanic connection between the conductive zone B and sediments, and reveals the asymmetry of the highly resistive upper crust whose resistivity changes from 283,000 Ωm in the north to 13,000 Ωm in the south (in the initial TS model, from 100,000 Ωm in the north to 10,000 Ωm in the south).

The TM model is the final model obtained from the successively applied automatic partial inversions. Its agreement with the initial TS model is evident. All of the major TS structures are well resolved in the TM model. Misfits between these models do not exceed 5–7% in tippers and 2.5° in phases.

For comparison, Figure 2.9 presents the PI model, obtained by the parallel (joint) inversion of all response functions ($\mathrm{Re}W_{zy}$, $\mathrm{Im}W_{zy}$, $\varphi^{\parallel}$, $\rho^{\perp}$, and $\varphi^{\perp}$)

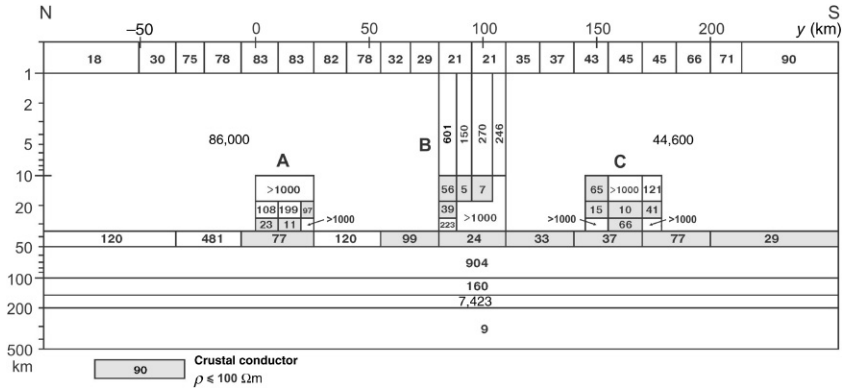

FIGURE 2.9 The PI model: Parallel inversion of ReW_{zy}, ImW_{zy}, $\varphi^{\parallel}$, $\rho^{\perp}$, and $\varphi^{\perp}$ using the II2DC code; the resistivity values in Ωm are shown within blocks; blocks of lower crustal resistivities are shaded (cf. Figure 2.3).

used in constructing the TM model (the starting model was the same as in the tipper inversion). In the PI model: (1) resistivity contrasts in the sedimentary cover are significantly smoothed, (2) the resistivity contrast in the upper, highly resistive crust is also significantly smoothed, (3) the conducting zones A and C are resolved with some degree of certainty, but the central through-the-crust conducting zone B is completely destroyed, (4) the contrast between the two edge resistivities in the crustal conducting layer is much lower, and (5) the monotonic decrease of the mantle resistivity is disturbed (a poorly conducting layer appears in the conducting mantle). We see that the parallel inversion of all response function used impairs the interpretation result.

Of course, the parallel inversion is the simplest approach to a multicriterion problem, and apparently this is the reason why it is popular among geophysicists fascinated by the possibility of automatic inversions eliminating the necessity of comprehensive analysis. The transition to the technique of SPI undoubtedly complicates the work, and this is a possible reason for the objections raised in the discussions. However, our experiments on the integrated interpretation of MV and MT data indicate that the game, albeit more difficult, is worth the candle.

2.4 MV–MT STUDY OF THE CASCADIAN SUBDUCTION ZONE (EMSLAB EXPERIMENT)

The above scheme of SPI of MV and MT data was applied in constructing the geoelectric model for the Cascadian subduction zone (Wannamaker et al., 1989a; Vanyan et al., 2002). We used data obtained in 1986–1988 by geophysicists from the United States, Canada, and Mexico on the Pacific North American coast within the framework of the experiment "Electromagnetic sounding of lithosphere and asthenosphere beneath (the Juan de Fuca plate)" (EMSLAB).

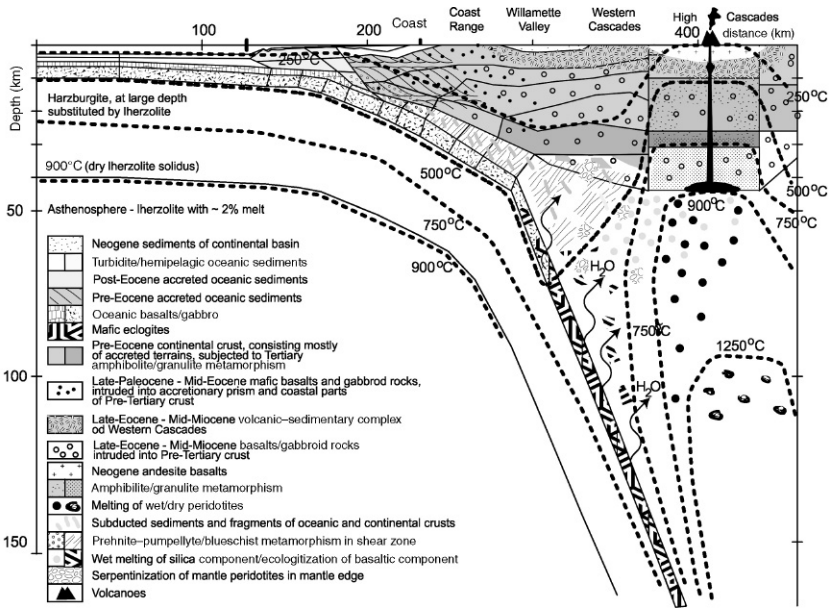

FIGURE 2.10 Predictive geothermal and petrological CASCADIA model constructed along an E-W profile across central Oregon (Romanyuk et al., 2001).

Figure 2.10 presents a predictive petrological and geothermal model of the Cascadian subduction zone along an E-W profile generalizing modern ideas and hypotheses on the structure of the region and its fluid regime (Romanyuk et al., 2001). The subducting Juan de Fuca plate originates at an offshore spreading ridge (about 500 km from the coast). In the eastward direction, the profile crosses (1) an abyssal basin with a sedimentary cover 1–2 km thick and a pillow lava layer 1.5–2 km thick; (2) the Coast range, formed by volcanic-sedimentary rocks; (3) the Willamette river valley, filled with a thick sequence of sediments and basaltic intrusions; (4) the Western (older) and Eastern (younger) Cascade ranges, consisting of volcanic and volcanic-sedimentary rocks typical of a recent active volcanic arc; and (5) the Deschutes Plateau, covered with lavas.

The abyssal basin is characterized by a typical oceanic section with the asthenosphere at a depth of about 40 km (the 900°C isotherm). The continental crust above the subducting slab has lower temperatures. A subvertical zone of higher temperatures reaching the melting point of wet peridotite (~900°C) has been localized beneath the high Cascades. The release of fluids from the upper part of the slab appears to be due to a few mechanisms. First, at depth to about 30 km, free water is released from micropores and microfractures under the action of the increasing lithostatic pressure. Dehydration of minerals such as talc, serpentine, and chlorite starts at depths of 30–50 km, where the temperature exceeds 400°C. Finally, the basalt–eclogite transition can start at depth greater than 75 km, and exsolution of amphibolites can take place at depths of

more than 90 km. All these processes are accompanied by the release of fluids. Supposedly, fluids released at small depths migrate through the contact zone between the oceanic and continental plates. At greater depths, fluids can be absorbed by mantle peridotites (serpentinization). They disturb the equilibrium state of material and cause "wet" melting. The melts migrate upward toward the Earth's surface, producing a volcanic arc.

Two 2-D geoelectric models of the Cascadian subduction zone constructed along the Lincoln line (an E-W profile in the middle part of Oregon) have been discussed in the literature: EMSLAB-I (Wannamaker et al., 1989b) and EMSLAB-II (Varentsov et al., 1996).

The EMSLAB-I model, shown in Figure 2.11, was constructed by a trial-and-error method with a strong priority given to the TM mode (the latter, in the opinion of the authors of this model, is least subjected to 3-D distortions). The EMSLAB-I model minimizes the misfits of the curves $\rho^{\perp}$ and $\varphi^{\perp}$ and ignores the curves $\rho^{\parallel}$ and $\varphi^{\parallel}$. Its main elements are (1) the upper conductive part of the plate, sinking at a low angle beneath the Coast range, (2) a subhorizontal conducting layer in the middle continental crust broadening in the area of the High Cascades, and (3) a well developed conductive asthenosphere beneath the ocean. The problem of the junction between the slab and the crustal conductor remains open in this model. The continental asthenosphere is ignored, although the shape of the experimental curves $\rho^{\parallel}$ and $\varphi^{\parallel}$ suggested a low resistivity of the upper mantle. The absence of catching the eye divergences between the model values of $\mathrm{Re}W_{zy}$ and $\mathrm{Im}W_{zy}$ and the experimental data is considered by the authors as evidence of the reliability of the model.

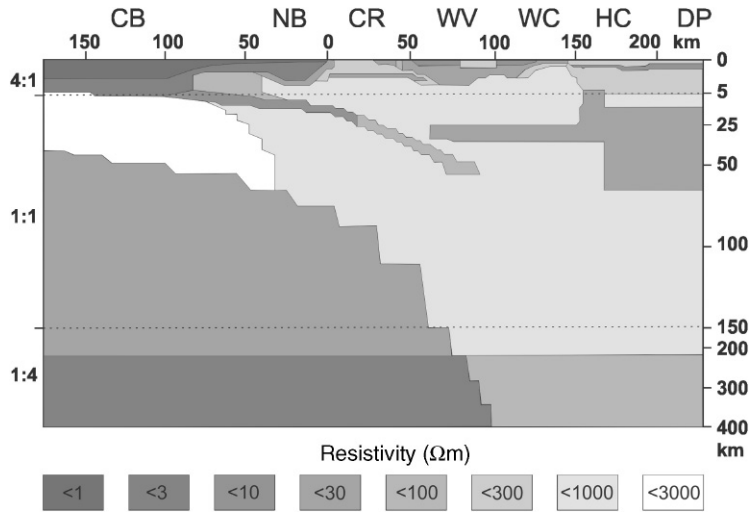

FIGURE 2.11 Geoelectric 2-D model EMSLAB-I of the Cascadia subduction zone (Wannamaker et al., 1989b); CB, Cascadia Basin; NB, Newport Basin; CR, Coast Range; WV, Willamette Valley; WC, Western Cascades; HC, High Cascades; DP, Deschutes Plateau.

The EMSLAB-I model is vulnerable to criticism. A cold continental mantle contradicts current geodynamic ideas of the Cascadian subduction zone (compare the EMSLAB-I model with the predictive CASCADIA model shown in Figure 2.10). Analysis of the EMSLAB-I model has shown that the TM mode is weakly sensitive to variations in the electric conductivity of the mantle and that the bimodal inversion alone, using both the TE and TM modes, can be effective in studying the asthenosphere (Vanyan et al., 2002).

Experiments on the bimodal interpretation of MT and MV data obtained in the Cascadian subduction zone resulted in the 2-D EMSLAB-II model (Figure 2.12). It was constructed with the automatic inversion code INV2D-FG, optimizing resistivities on 20 blocks of a fixed geometry (Varentsov et al., 1996). An algorithm of parallel weighted inversion was applied to $\varphi^{\perp}$, $\mathrm{Re}W_{zy}$ and $\mathrm{Im}W_{zy}$ (maximum weight), $\varphi^{\parallel}$ and $\rho^{\perp}$ (normal weight), and $\rho^{\parallel}$ (minimum weight). The EMSLAB-II model has much in common with EMSLAB-I. Both have the same oceanic asthenosphere, subducting slab, and crustal conducting layer. However, the EMSLAB-II subducting plate joins the crustal conductor, and a conducting asthenosphere is present in the continental mantle. Thus, the geoelectric data have revealed partial melting in the continental mantle. The main drawback of the EMSLAB-II model is its sketchiness due to the limited possibilities of the INV2D-FG code.

Presently, the INV2D-FG code has given way to more efficient software tools designed for the automatic 2-D inversion of MV and MT data. These are the smoothing code REBOCC (Siripunvaraporn and Egbert, 2000), the codes IGF-MT2D (Nowozynski and Pushkarev, 2001) and II2DC (Varentsov, 2002).

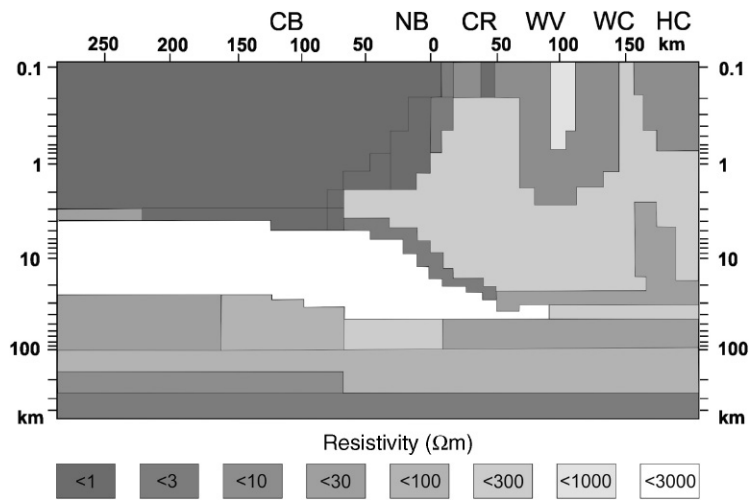

FIGURE 2.12 Geoelectric 2-D model EMSLAB-II of the Cascadian subduction zone (Varentsov et al., 1996); CB, Cascadia Basin; NB, Newport Basin; CR, Coast Range; WV, Willamette Valley; WC, Western Cascades; HC, High Cascades; DP, Deschutes Plateau.

The two last codes enable the optimization of models containing 512 and more blocks of a fixed geometry and provide new possibilities for interpreting the EMSLAB experimental data (Vanyan et al., 2002).

3-D model estimates obtained for the Pacific coast of North America and analysis of experimental data, induction arrows, and polar diagrams show that the regional structure along the Lincoln line is favorable for the 2-D interpretation of MV and MT data.

The interpretation consisted of three stages.

At the first stage, the 1-D inversion of short-period MT curves (T = 0.01–100 s) was performed and an approximate geoelectric section of the continental volcanic-sedimentary cover was constructed to a depth of 3.5 km. This section agrees with the near-surface portion of the EMSLAB-I model (Wannamaker et al., 1989b).

At the second stage, the REBOCC code was applied for the 2-D smoothed trial inversion. With the complicated conditions of the Cascadian subduction zone, the parallel inversion of the TE and TM modes yielded whimsical alternation of low- and high-resistivity spots with a poor minimization of the misfit. It is difficult to recognize real structures of the subduction zone in these spots. The most interesting result was obtained from the partial inversion of $\mathrm{Re}W_{zy}$, $\mathrm{Im}W_{zy}$, and $\varphi^{\parallel}$ (Figure 2.13). Here, the western and eastern conducting zones are separated by a T-shaped region of higher resistivity that can be associated with the subducting slab. An oceanic asthenosphere whose top can be fixed at a

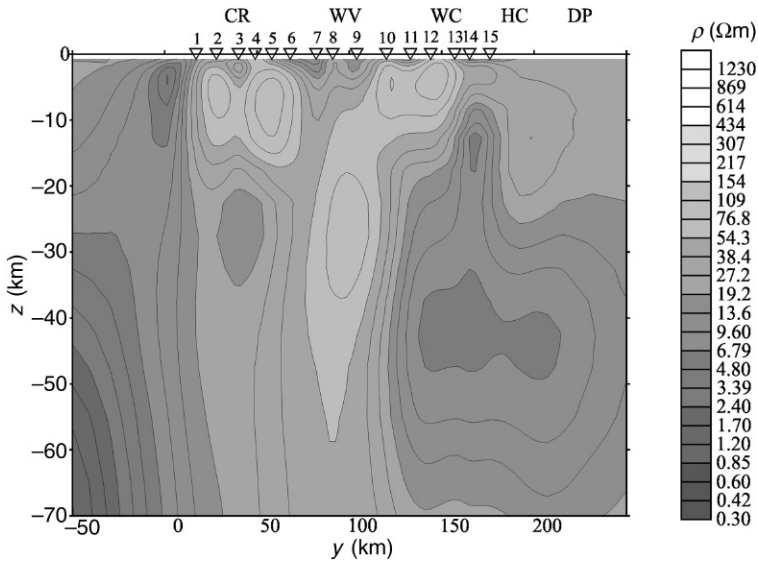

FIGURE 2.13 The trial model of the Cascadian subduction zone; 2-D inversion of $\mathrm{Re}W_{zy}$, $\mathrm{Im}W_{zy}$, and $\varphi^{\parallel}$ with the use of the smoothing REBOCC code; CR, Coast Range; WV, Willamette Valley; WC, Western Cascades; HC, High Cascades; DP, Deschutes Plateau.

depth of about 30 km is recognizable in the western conducting zone. The eastern conducting zone coincides with the crust-mantle zone of wet melting in the predictive CASCADIA model shown in Figure 2.10. It is noteworthy that the upper boundary of the eastern conductor closely resembles the topography of the crustal conducting zone in the EMSLAB-I and EMSLAB-II models shown in Figure 2.11.

At the third, final stage, the method of SPI was applied and a new 2-D geoelectric model of the Cascadian subduction zone was constructed (Vanyan et al., 2002). This model was called EMSLAB-III. It was constructed with the II2DC code (Varentsov, 2002) minimizing the model misfit in the class of media with a fixed geometry of blocks. The interpretation was conducted in the regime of testing hypotheses. We consider three hypothetic models of the Cascadian subduction zone: (1) CASCADIA predictive model, (2) EMSLAB-I model, and (3) EMSLAB- II model.

The interpretation model is shown in Figure 2.14. The ocean floor topography and thickness of the seafloor and shelf sediments were taken according to bathymetric and sedimentary thickness maps. The resistivities of the water, sediments, and oceanic crust are 0.3, 2, and 10,000 Ωm, respectively. The depth to the oceanic mantle and its resistivities were chosen in accordance with the CASCADIA, EMSLAB-I, and EMSLAB-II models. The slab surface was determined from seismic and seismic tomography data. The structure of the volcanic-sedimentary cover was specified from the 1-D inversion of short-period MT curves. The crust and mantle of the continent were divided into homogeneous

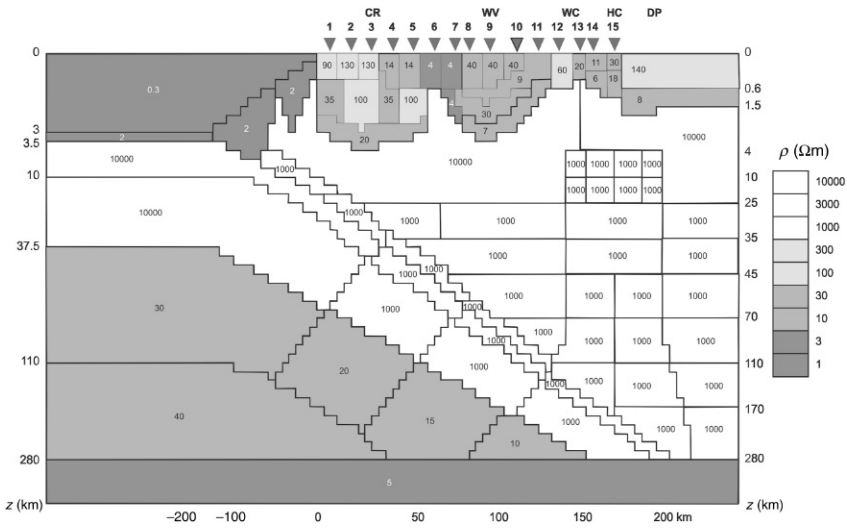

FIGURE 2.14 The interpretation block model; resistivity values of the initial START model are shown within blocks; CR, Coast Range; WV, Willamette Valley; WC, Western Cascades; HC, High Cascades; DP, Deschutes Plateau.

blocks. The division density and block geometry were chosen so that they admit a free choice of crust and mantle structures within the framework of the three hypotheses considered. A hypothesis best fitting the observed data can be chosen automatically in the process of misfit minimization. The continental crust and mantle have a resistivity of 1000 Ωm in the START model constructed on the basis of the interpretation model. We consider the SPI as:

1. Inversion of ReW_{zy} and ImW_{zy}. The START model was taken as the starting one. The TP model resulting from the inversion is shown in Figure 2.15. The tipper misfit (the RMS deviation of model tippers from observed values) in this model is 5–10 times smaller than the tipper amplitude (the difference between the maximum and minimum tipper values), which is an evidence of good agreement between the model and observations. A remarkable feature of the TP model is the conducting continental asthenosphere and the vertical low-resistivity zone that branches off the asthenosphere and crosses the continental crust in the High Cascade region. This feature distinguishes the TP model from EMSLAB-I and EMSLAB-II models and makes it similar to the predictive CASCADIA model, where a vertical high-temperature zone of wet and dry melting is evidently characterized by low resistivities.
2. Inversion of $\varphi^{\parallel}$. At this stage, we controlled the tipper inversion. To avoid difficulties associated with subsurface distortions of the curves $\rho^{\parallel}$, we confined ourselves to the inversion of the curves $\varphi^{\parallel}$, which satisfy the dispersion relations. The TP model, obtained from the tipper inversion, was used as a

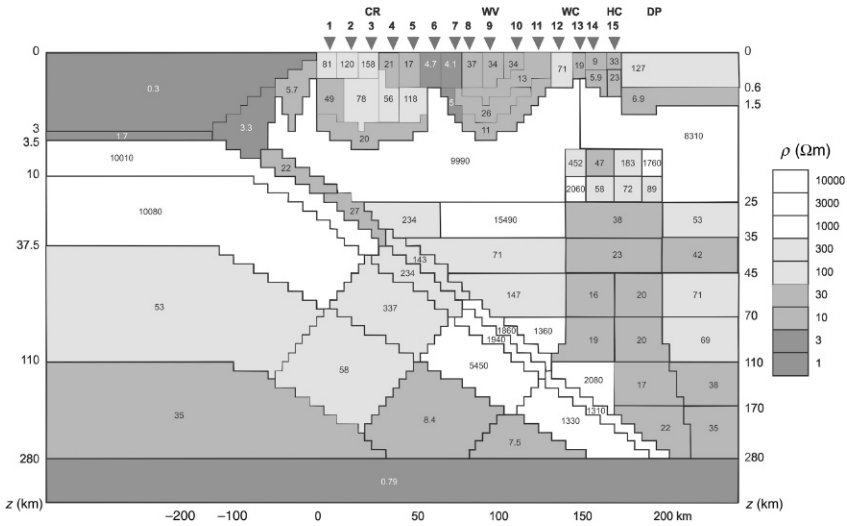

FIGURE 2.15 The TP model of the Cascadia subduction zone; 2-D inversion of ReW_{zy} and ImW_{zy} with the use of the block code II2DC (resistivity values in Ωm are shown within blocks); CR, Coast Range; WV, Willamette Valley; WC, Western Cascades; HC, High Cascades; DP, Deschutes Plateau.

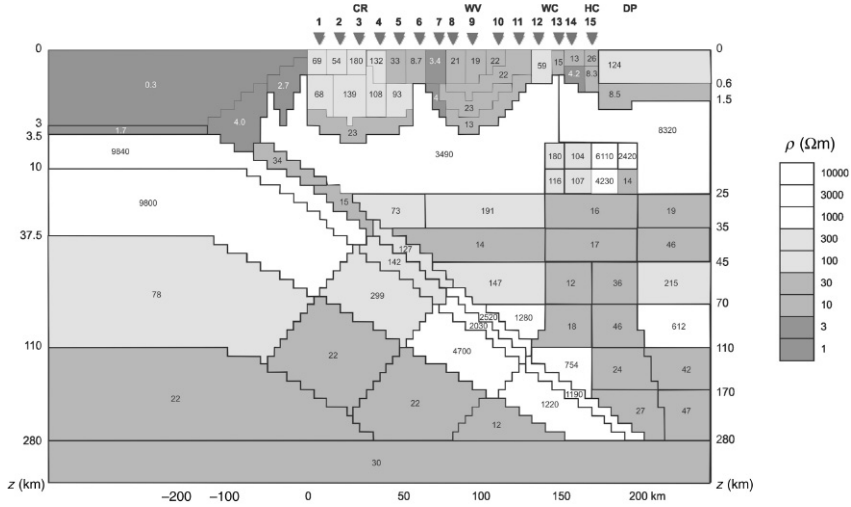

FIGURE 2.16 The TE model of the Cascadia subduction zone; 2-D inversion of $\varphi^{\parallel}$ with the use of the block code II2DC (resistivity values in Ωm are shown within blocks); CR, Coast Range; WV, Willamette Valley; WC, Western Cascades; HC, High Cascades; DP, Deschutes Plateau.

starting model. The inversion of longitudinal phases yielded the TE model, shown in Figure 2.16. The phase misfit (the RMS deviation of model phases from observed values) in this model is 5–10 times smaller than the phase amplitude (the difference between the maximum and minimum phase values), indicating good agreement of the model with observations. As distinct from the TP model, the TE continental crust includes a better delineated conducting layer (ρ = 14–46 Ωm) in a depth interval of 35–45 km, whereas the subvertical conducting zone (ρ = 12–46 Ωm) in a depth interval of 45–110 km, bounded by layers with resistivities of 147–1260 Ωm to the west and 215–612 Ωm to the east, is localized with a higher contrast. The TE model can be considered as an update of the TP model.

3. Inversion of $\rho^{\perp}$ and $\varphi^{\perp}$. At this stage, we inverted the TM mode, which is less sensitive to conducting zones in the crust and mantle but is more effective in resolving the structure of the junction zone between the slab and crustal conducting layer. Besides, it provides more reliable estimates of the resistivity in the upper consolidated crust. In inverting the TM mode, the TE model, obtained from the inversion of phases $\varphi^{\parallel}$, was taken as a starting model. The inversion of transverse apparent resistivities and phases of the transverse impedance yielded the TM model shown in Figure 2.17. In this model, the misfits of transverse apparent resistivities at most points vary within 6–12%, and the phase misfits are 7–10 times smaller than the phase amplitude (the difference between the maximum and minimum phase values). The TM model inherits the main features of the starting TE model (albeit with some

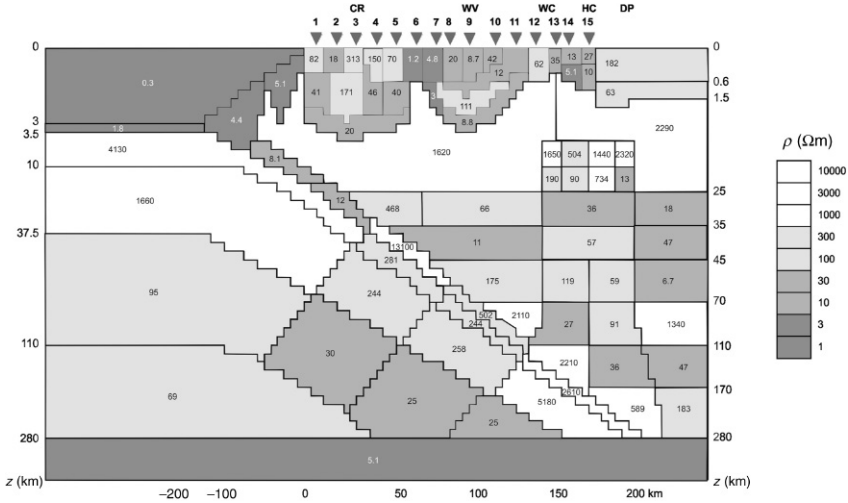

FIGURE 2.17 The TM model of the Cascadia subduction zone; 2-D inversion of $\rho^{\perp}$ and $\varphi^{\perp}$ with the use of the block code II2DC (resistivity values in Ωm are shown within blocks); CR, Coast Range; WV, Willamette Valley; WC, Western Cascades; HC, High Cascades; DP, Deschutes Plateau.

deviations). The following implications of the TM model are noteworthy. First, no well-conducting junction is present between the conducting slab and the crustal conducting layer. Second, the upper consolidated crust of the continent has a resistivity of about 2000 Ωm, indicating that it is fractured.

4. Synthesis. At this stage, we analyzed the TP, TE, and TM models and constructed the generalized EMSLAB-III model, smoothing insignificant details and enlarging blocks. All changes were made interactively with the calculation of local misfits and the correction of boundaries and resistivities. The resulting model shown in Figure 2.18 provides a coherent geoelectric image of the subduction zone. The extent of its agreement with observed data is seen from Figure 2.19, where the model curves $\rho^{\perp}$, $\rho^{\parallel}$, $\varphi^{\perp}$, $\varphi^{\parallel}$, $\mathrm{Re}W_{zy}$, and $\mathrm{Im}W_{zy}$ are compared with the observed curves (the static distortion in the observed $(^{\parallel}$ curves was removed by a vertical shift of their low-frequency branches). The model curves agree well with the observed curves at the majority of sites.

In its oceanic part, the EMSLAB-III model is close to EMSLAB-I and EMSLAB-II models and exhibits a thick oceanic asthenosphere in a depth interval of 37.5–110 km.

The structure of the continental part of EMSLAB-III is distinguished by the following significant elements: (1) a crustal conducting layer (ρ = 20 Ωm, a depth interval of 25–40 km) and a conducting asthenosphere (ρ = 30 Ωm, a depth interval of 100–155 km) are distinctly resolved, (2) crustal and asthenospheric conductors are connected by a column-like conducting body

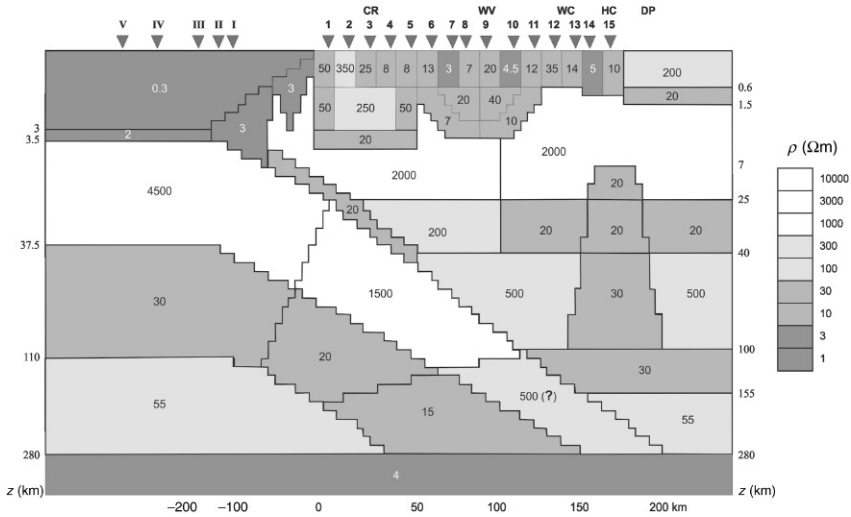

FIGURE 2.18 The final EMSLAB-III model (resistivity values in Ωm are shown within blocks); I–V, soundings on the ocean floor; 1–15, soundings on the continent; CR, Coast Range; WV, Willamette Valley; WC, Western Cascades; HC, High Cascades; DP, Deschutes Plateau.

(ρ = 20–30 Ωm) crossing the lithosphere and reaching depths of about 7 km in the volcanic zone of the High Cascades, (3) a subducting slab, in a depth interval of 4–40 km contains a thin inclined conductor (ρ = 20 Ωm) separated from the crustal conducting layer by a higher-resistivity zone (ρ = 60 Ωm); apparently, the crustal conducting layer has a deep origin.

The reliability of these elements is supported by the fact that the elimination of any of them noticeably increases the model misfits.

These features of the continental section make the EMSLAB-III and predictive CASCADIA models similar. The fluid regime of the subduction can be clearly observed here. The subducting slab entraps fluid-saturated low-resistivity rocks of the ocean floor. As the slab moves down, the released free water migrates through the shear zone (the contact zone between the subducting oceanic and stable continental plates). The dehydration (the release of bound water) developing in the slab at depths of 30–40 km supplies fluids to the mantle and causes the wet melting of asthenospheric material. The low-resistivity melts move upward through the lithosphere and form a volcanic arc. The heating of the lithosphere activates dehydration in the lower crust, producing the crustal conducting layer.

Thus, using the MV–MT complex with MV priority, we managed to construct a meaningful geodynamic model of the Cascadian subduction and successfully complete the EMSLAB experiment. It seems that the development of the MV method should be regarded as a promising task of modern geophysics.

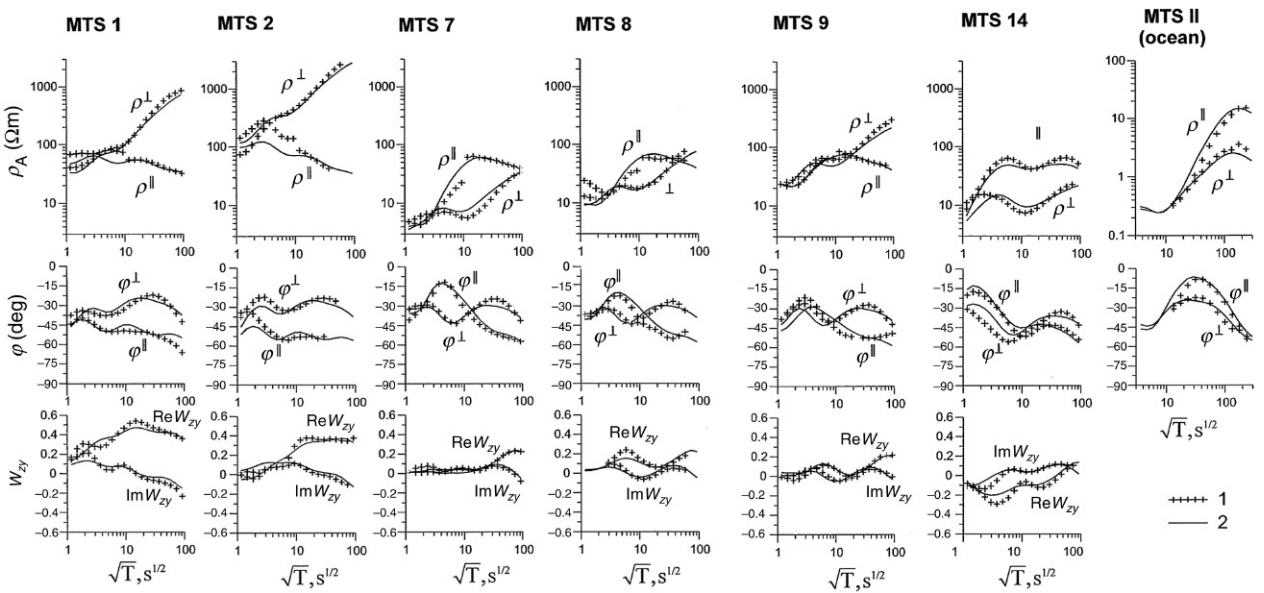

FIGURE 2.19 Comparison of the observed MT and MV curves with the curves calculated from the EMSLAB-III model: (1) observations, (2) EMSLAB-III model.

ACKNOWLEDGMENTS

We are grateful to P. Weidelt and U. Schmucker for discussions stimulating this work. The work was supported by the Russian Foundation for Basic Research, projects 05-01-00244 and 05-05-65082.

REFERENCES

Berdichevsky, M.N., Dmitriev, V.I., 2002. Magnetotellurics in the Context of the Theory of Ill-Posed Problems. SEG monograph, Tulsa, p. 215.

Berdichevsky, M.N., Dmitriev, V.I., Pozdnjakova, E.E., 1998. On two-dimensional interpretation of magnetotelluric soundings. Geophys. J. Int. 133 (3), 585–606.

Berdichevsky, M.N., Vanyan, L.L., Koshurnikov, A.V., 1999. Magnetotelluric sounding in the Baikal Rift Zone. Izv. Phys. Solid Earth 35 (10), 793–814.

Berdichevsky, M.N., Dmitriev, V.I., Golubtsova, N.S., Mershchikova, N.A., Pushkarev, P.Yu., 2003. Magnetovariational sounding: new possibilities. Izv. Phys. Solid Earth 39 (9), 701–727.

Nowozynski, K., Pushkarev, P.Yu., 2001. The efficiency analysis of programs for two-dimensional inversion of magnetotelluric data. Izv. Phys. Solid Earth 37 (6), 503–516.

Pous, J., Queralt, P., Marcuello, A., 2001. Magnetotelluric signature of the Western Cantabrian Mountains. Geophys. Res. Lett. 28 (9), 1795–1798.

Roecker, S.W., Sabitova, T.M., Vinnik, L.P., Burmakov, Y.A., Golovanov, M.I., Mamatkhanova, R., Munirova, L., 1993. Three-dimensional elastic wave velocity structure of Western and Central Tien Shan. J. Geophys. Res. 98 (B9), 15579–15795.

Rokityansky, I.I., 1982. Geoelectromagnetic Investigations of the Earth's Crust and Mantle. Springer, Berlin, p. 381.

Romanyuk, T.V., Mooney, W.D., Blakely, R.J., 2001. A tectonic-geophysical model of the Cascadian subduction zone in North America. Geotektonika 3, 88–110.

Simpson, F., Bahr, K., 2005. Practical Magnetotellurics. Cambridge University Press, Cambridge.

Siripunvaraporn, W., Egbert, G., 2000. An efficient data subspace inversion method for 2-D magnetotelluric data. Geophysics 65, 791–803.

Trapeznikov, Yu.A., Andreeva, E.V., Batalev, V.Yu., Berdichevsky, M.N., Vanyan, L.L., Volykhin, A.M., Golubtsova, N.S., Rybin, A.K., 1997. Magnetotelluric soundings in the mountains of the Kirghyz Tien-Shan. Izv. Phys. Solid Earth 1, 3–20.

Vanyan, L.L., Berdichevsky, M.N., Pushkarev, P.Yu., Romanyuk, T.V., 2002. A geoelectric model of the Cascadia subduction zone. Izv. Phys. Solid Earth 38 (10), 816–845.

Varentsov, I.M., 2002. A general approach to the magnetotelluric data inversion in a piecewise-continuous medium. Izv. Phys. Solid Earth 38 (11), 913–934.

Varentsov, I.M., Golubev, N.G., Gordienko, V.V., Sokolova, E.Yu., 1996. Study of the deep geoelectric structure along the Lincoln Line (EMSLAB Experiment). Izv. Phys. Solid Earth 4, 124–144.

Wannamaker, P.E., Stodt, J.A., Rijo, L., 1987. A stable finite element solution for two-dimensional magnetotelluric modeling. Geophys. J. R. Astron. Soc. 88, 277–296.

Wannamaker, P.E., Booker, J.R., Filloux, J.H., Jones, A.G., Jiracek, G.R., Chave, A.D., Tarits, P., Waff, H.S., Young, C.T., Stodt, J.A., Martinez, M., Law, L.K., Yukutake, T., Segava, J.S., White, A., Green, A.W., 1989a. Magnetotelluric observations across the Juan de Fuca subduction system in the EMSLAB project. J. Geophys. Res. 94 (B10), 14111–14125.

Wannamaker, P.E., Booker, J.R., Jones, A.G., Chave, A.D., Filloux, J.H., Waff, H.S., Law, L.K., 1989b. Resistivity cross-section through the Juan de Fuca subduction system and its tectonic implication. J. Geophys. Res. 94 (B10), 14127–14144.